

Liquid-level Sensor Using Embedded Fiber Bragg Grating in CFRP Diaphragm

Ademir Carlos Nicolini Junior¹, Jessé de Pelegrin², Gustavo Gomes Kuhn¹, Cicero Martelli³, Jean Carlos Cardozo da Silva³, Uilian José Dreyer³, Kleiton Moraes Sousa¹.

¹Federal University of Parana, Brasil - Pato Branco. Correspondent author: Kleiton M. Sousa
(kleitonsousa@utfpr.edu.br)

²Instituto Federal Catarinense - Luzerna

³Federal University of Parana, Brasil - Curitiba

Abstract— This article presents the development of a liquid-level sensor using fiber optic Bragg gratings (FBG). The sensor comprises a carbon-fiber-reinforced polymers (CFRP) diaphragm packaging an embedded FBG to measure strain. A mathematical analysis determines the FBG response to the pressure exerted by a liquid column over the packaged sensor. The experimental arrangement consists of an acrylic tube with a sensor at the bottom. FBG signals were acquired using a DI 410 optical interrogator manufactured by HBM. A finite element simulation with Ansys was performed to determine the most reposeful position from the FBG sensor. The experimental results show the analysis of eight repetitions of the water column ranging from 10 cm to 60 cm using 10 cm steps. The sensor showed a linear response, with a coefficient of determination of 0.999, and a sensitivity of 4.1 pm/cm; and the maximum standard deviation is 0.64 pm. Although water is used in the calibration process, other liquids could also be used, obtaining a different angular coefficient depending on the density of the liquid used.

Index Terms— Carbon-fiber-reinforced polymers, embedded optical fiber sensor, fiber Bragg grating, liquid-level sensor.

I. INTRODUCTION

The measurement of physical quantities plays a role of great importance for industrial activity. Physical parameters such as temperature, pressure, level, and deformation are of fundamental importance to ensure adequate control and supervision of industrial processes. For most of these applications, conventional electrical and electronic sensors perform satisfactorily. However, there are limiting situations for conventional sensors that compromise the measured value. Such factors include electromagnetic interference, the distance between the sensor and the processing unit, or the number of measurement points. In situations of this type, it is necessary to investigate new measurement methods, and in this scenario, optical sensors are an alternative to conventional electrical sensors [1]–[3].

Fiber Optic Bragg gratings (FBG) stand out among the types of optical sensors [4]. FBGs are used in telecommunication systems for laser stabilization, signal multiplexing, dispersion compensation, and optical filters [5]. However, the intrinsic sensitivity of FBGs for measuring temperature and strain led to their application as a sensor. Thus, it was possible to unite the need to measure physical quantities together with the inherent characteristics of the optical fiber [2]. The main characteristics of FBGs for use as a sensor are a passive sensor, not requiring power for its operation; small mass, which ensures a response in the order of milliseconds for temperature and strain measurements; measurement carried

out in wavelength, with this it is possible the multiplexing of several sensors in the same optical fiber; immune to electromagnetic interference, since the optical fiber is composed of silica and does not conduct electricity; low signal loss, in the order of 0.2 dB/km in the 1.5 μm spectrum region [6].

Due to their characteristics, FBG sensors have a wide range of applications, especially immunity to electromagnetic interference; their application in electrical machines and power distribution systems stands out. In [7], the temperature measurement and validation of a thermal model of a three-phase induction motor is presented. Still, in the application in induction motors, FBGs sensors are used for fault diagnosis in rotors [8] and bearings [9]. In [10], a pattern recognition technique is presented to identify bearing failures in induction motors based on the measurement performed by an FBG. In [11] is presented a measurement technique to identify the different eccentricities of induction motors due to unbalanced magnetic pull. Still, about electrical machines, FBG sensors are used for temperature measurements [12] or even simultaneous measurement of temperature and vibration in hydrogenerators [13].

FBGs are also used prominently in biomedical engineering applications. In [14], a study using FBG sensors glued to Schanz pins evaluated the evolution of bone, where three materials of different densities were inserted into the fracture site (synthetic femur) to simulate the formation of bone callus is presented. Socorro-Leranz *et al.* [15] report the development and characterization of parallel FBG to monitor the movements of the wrist and fingers of a hand, the system that can be used to monitor the positions of the hand or for the rehabilitation of patients suffering from neuromotor or post-stroke diseases. Kalinowski *et al.* [16] used FBG sensors to measure the static and dynamic strain of the external fixation device used in patients who have suffered fractures in the lower limbs. In [17], the authors use four FBG sensors embedded in carbon fiber-reinforced polymer in a smart foot; the results of the FBG sensors are used in an adaptive fuzzy-proportional–integral–derivative (FPID) control strategy.

Liquid level monitoring is essential in the industry for many reasons, including evaluating the stock of storage tanks, preventing overflows and leaks, reducing waste and downtime, and improving safety and regulatory compliance [18]. There are several methods for monitoring liquid levels. Some of the most common methods include differential pressure transmitters that measure the hydrostatic pressure of a liquid in a tank or reservoir and convert that pressure into an electrical signal that can be read by a controller or gauge [19]. Load cells measure the force the liquid exerts on a specific point in the tank or reservoir. This force is then converted into an electrical signal that a controller can read [20]. At least using radar technology is a non-contact method that involves sending an electromagnetic pulse to the surface of a fluid and measuring the time required for the pulse to return to the sensor. The faster the pulse returns, the higher the fluid level [21].

Previous papers demonstrated several ways to measure liquid levels with different types of FBGs and encapsulation techniques, and some of these techniques are summarized in [22]. One way to use FBGs as a level sensor is to determine the refractive index of the medium surrounding the sensor. The refractive index changes as the water column rise and comes into contact with the sensor. In [23], a level sensor using an etched chirp FBG is used as a level sensor. In [24], tilted FBGs are used as a refractive index sensor. Another way to measure the refractive index is using long-period gratings (LPG) [25], [26]. This type of liquid-level sensor has the disadvantage that the sensor is exposed to the environment, which can make it fragile.

One way to perform the level measurement is from an indirect measure, such as the deformation of a

diaphragm. This diaphragm acts as an encapsulation for the FBG and keeps it protected from mechanical impacts. Different materials and techniques can be used to make the diaphragm. In [27], the authors present a rubber diaphragm with an FBG sensor glued in the center of this diaphragm. In [28], the material used in the diaphragm is epoxy, with an FBG embedded. In [29], a liquid-level sensor system is presented based on a pair of FBG embedded in a circular silicone (PDMS—polydimethylsiloxane) rubber diaphragm. The pair of sensors in [29] were used to compensate for the cross-sensitivity to temperature and strain of the FBG sensor.

One of the materials that have been gaining attention for encapsulating FBG sensors is carbon fiber reinforced composite (CFRC) [30]. Sensors with an FBG embedded in CFRC were used to measure strain in transformers [31], to identify faults in electric motors [9], and also to develop liquid-level sensors [32] using two sheets of CFRC diaphragm and an FBG sensor glued between them.

This article presents the development, finite element modeling, and calibration of a liquid-level sensor using a CFRC diaphragm with an embedded FBG. The manufacturing method, with an embedded FBG, contributes to this work.

II. MATERIALS AND METHODS

A. Sensor Analysis and Development

Fig. 1 presents an illustration of the developed sensor. The main dimensions of the sensor are also shown in Fig. 1. The sensor comprises a carbon fiber diaphragm positioned on a stainless steel flange with an embedded FBG. The upper part of the flange has a threaded connection to the water tank, compatible with pipes used in industrial hydraulic systems.

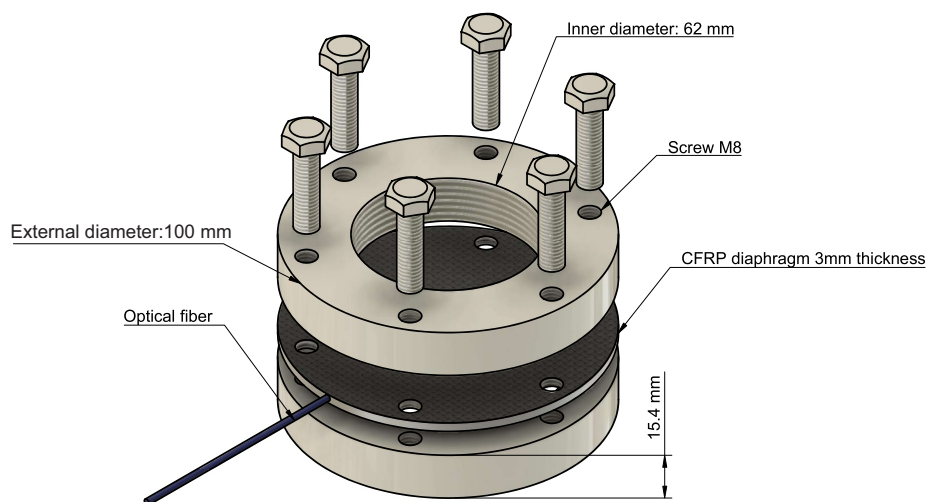


Fig. 1. Liquid-level sensor and its dimensions.

The water column exerts a uniform pressure on the diaphragm, and this, in turn, presents an axial and radial deformation, which can be represented by [28], [32]:

$$\varepsilon_t = \frac{3P}{8Et^2} (1 - \nu^2) (R - r^2), \quad (1a)$$

$$\varepsilon_r = \frac{3P}{8Et^2} (1 - \nu^2) (R - 3r^2), \quad (1b)$$

where E is Young's module, R is the diaphragm radius, ν is Poisson's coefficient (0.5 for CFRP [28]), t is the thickness, r the distance from the point where the strain is measured to the center of the diaphragm, and P is the applied pressure. The applied pressure due to a column of liquid can be determined by:

$$P = dgh, \quad (2)$$

where d is the liquid density, g is the acceleration of gravity and h is the height of the liquid column. In this paper, the sensor is characterized using water whose density is 997 kg/m^3 . The FBG suffers only the effect of the radial deformation ϵ_r and, according to (1b), the greatest deformation point is in the diaphragm's center (when $r = 0$). Because of this, the diaphragm is manufactured with the FBG in the center.

The Bragg wavelength λ_B is sensitive to the effective refractive index and the grating period. Changing one of these two parameters resulting from external interference causes a shift $\Delta\lambda_B$ in the value of the central wavelength reflected by the FBG (λ_B). The mechanical and thermal changes of the medium are related to the displacement $\Delta\lambda_B$ using the expression [2]:

$$\Delta\lambda_B(\Delta\epsilon, \Delta T) = \lambda_B[(1 - p_e)\Delta\epsilon + (\alpha_n + \alpha_\Lambda)\Delta T], \quad (3)$$

where ΔT is the temperature variation and $\Delta\epsilon$ is the strain variation experienced by FBG. Still in (3), p_e is the effective photoelastic constant, α_Λ is the thermal expansion coefficient for the fiber and α_n thermo-optic coefficient. For an FBG with a central wavelength of 1550 nm, (3) yields the expected sensitivity of $1.2 \text{ pm}/\mu\epsilon$ for strain variation and $10 \text{ pm}/^\circ\text{C}$ for temperature variation [2].

From (3), one can see that it is necessary to compensate for the temperature variation when the only strain measurement is desired. In this paper, the compensation is performed using an encapsulated FBG in an alumina tube that is in contact with the water column. The FBG has Bragg resonance peak wavelength of 1532 nm, full width half maximum of 0.3 nm and about 50 % reflectivity. The encapsulation ensures that the FBG is subject only to temperature variations.

Substituting (1b) in the first installment of (3), considering a level variation Δh :

$$\Delta\lambda_B = \overbrace{\lambda_B[(1 - p_e)]}^{1.2 \text{ pm}/\mu\epsilon} \underbrace{\frac{3dg\Delta h}{8Et^2}(1 - \nu^2)}_{\Delta\epsilon} R, \quad (4)$$

and (4) is used to obtain the Bragg wavelength variation of the liquid-level sensor. In (4), it is possible to identify the parameters that can modify the deformation experienced by the FBG. The deformation is directly proportional to the density of the liquid used. Therefore, increasing the density of the liquid is expected to obtain a greater deformation. This paper uses water to obtain the sensor response.

Still, about (4), the thickness of the diaphragm is inversely proportional to the deformation, being a quadratic relationship. For a higher sensibility, this thickness should be as small as possible. Young's module is also inversely proportional to the deformation, but this parameter is intrinsic to the material used and cannot be changed.

B. Experimental Setup

The liquid level sensor consists of an embedded FBG to measure the strain of a CFRP diaphragm. An uniform FBG sensor is used for strain measurement, recorded using the phase mask technique onto a Ge-doped photosensitive fiber. The FBG was written using an excimer laser (Xantos XS 500 - 193 nm-XS-L Coherent) with 193 pulsed emission up to 500 Hz and wavelength at 193 nm. The phase mask period used is 1060 nm, resulting in a Bragg wavelength centered at 1533 nm, with a reflectivity of 80%. The FBG recording was made at the Multiuser Photonics Laboratory of the Federal University of Technology – Parana at Curitiba.

The optical fiber was embedded between two layers of carbon fiber composite of bidirectional and unidirectional carbon fiber (200 g/m^2) and epoxy resin (331), and term with hardening (043), manufactured by Dow Chemical Company. The first layer of carbon fiber was impregnated with epoxy resin, sealed hermetically, and subjected to a healing process at elevated temperature. The optical fibers with the FBG sensors were positioned under the first layer and covered by the second layer. To ensure a high-quality product, a vacuum pump was used to remove air particles during the curing process, which was performed at $120 \text{ }^\circ\text{C}$ for 8 hours. According to (4), to get the maximum wavelength variation, the CFRP diaphragm must have the lowest possible thickness. However, given the manufacturing process, the lowest thickness obtained is 3 mm.

Fig. 2 presents the experimental setup used to obtain the sensor response. For a calibration of the used sensor an acrylic tube 1 m high. At the bottom of the tube a valve was placed to reduce the water level when necessary. An optical interrogator DI-410, manufactured by HBM, with four input channels and an acquisition rate of 1 Hz reads the FBG sensor. HBM's Catman[®] Easy software collects the optical interrogator data.

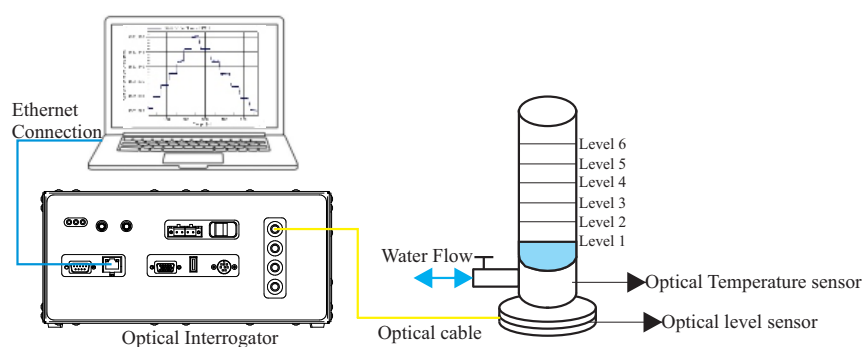


Fig. 2. Experimental Setup.

III. RESULTS AND DISCUSSIONS

A. Finite Element Analysis and Simulation

Equations (1a) and (1b) present the deformation suffered by a diaphragm. Inspection of these equations leads to the conclusion that the value of r must equal zero to obtain the most significant deformation. Since r is the distance of the analyzed point to the center of the diaphragm, the most significant deformation occurs at the center, when $r = 0$. A finite element simulation is performed to demonstrate that the center of the diaphragm is, in fact, the place with the most significant deformation. The simulation consists of applying a normalized pressure of 1 MPa. The simulation must be performed

for a pressure input since this is the physical quantity experienced by the diaphragm when it is under a column of liquid.

The simulation result is presented in Fig. 3. The software ANSYS 2022R1 Researcher was used and had 34524 nodes and 18393 elements. The place with the most significant deformation is in the center of the diaphragm, with a value of 0.02742 mm for a pressure of 1 MPa, which corroborates what is expected by (1a) and (1b). Thus, the installation location of the FBG so that the sensitivity of the level sensors is the best possible must be the center of the CFRP diaphragm.

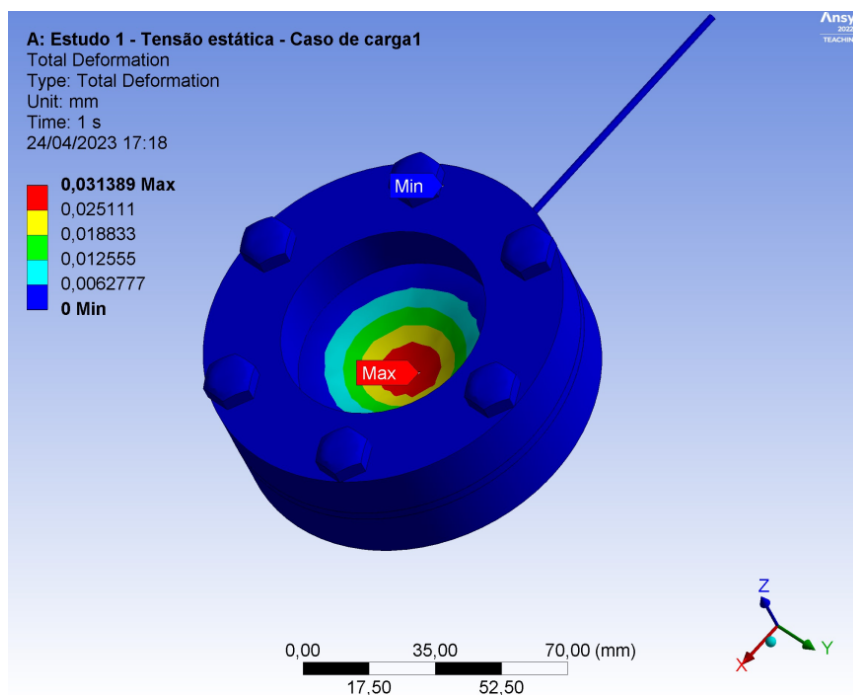


Fig. 3. Deformation FEM simulation of the CFRP diaphragm.

B. Sensor calibration

The tests were conducted in a room with a controlled temperature of 23 °C. The calibration occurred as follows: water column variations of 10 cm, with a maximum level of 60 cm. A total of 8 repetitions were performed. Fig. 4 shows the response of the liquid-level sensor. The sensor has a linear response, with a correlation coefficient of 0.999 and an angular coefficient of 4.1 pm/cm. The integration of FBG and CFRP produced a linear response and protected the sensor from mechanical impacts. Since the liquid used in this paper is water, each variation of 10 cm in the water column is equivalent to a pressure variation of 984.04 Pa, and the maximum pressure applied to the sensor is 5904.2 Pa. Although the sensor was calibrated against the height of the water column, it can also be used as a pressure sensor. The variation in wavelength depends, in addition to the height of the water column, on the liquid being used. Changing the liquid used would change the applied pressure, and if the liquid has a greater density than water, the sensor response would have a linear coefficient greater than that obtained with water.

Table I presents the mean values of Bragg wavelength variation. The variation in wavelength between each 10 cm step is similar for all values, about 4 pm, which indicates the sensor's linear response. The maximum standard deviation observed was 0.64 pm, and this standard deviation value is mainly due to

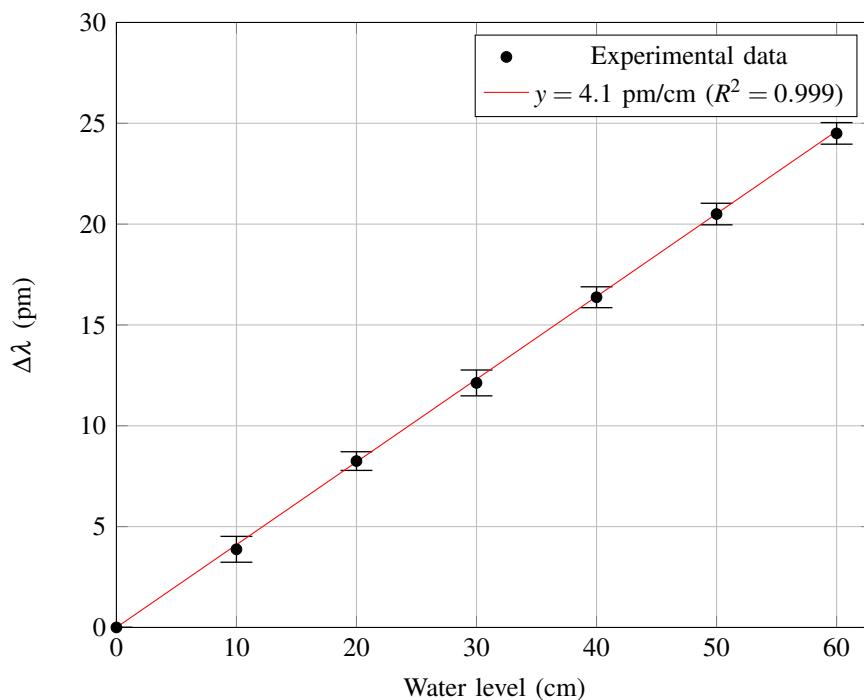


Fig. 4. Liquid-level sensor calibration response.

the calibration process performed. Small variations in the poured liquid amount inside the tube can lead to greater standard deviation values. That is the case when draining the liquid using the manual valve positioned in the tube's base. Despite this, the linear correlation coefficient was $R^2 = 0.999$, confirming the sensor's linear response.

TABLE I. Mean values obtained by calibrating the level sensor and the standard deviation for each water column height value.

Water level (cm)	Mean $\Delta\lambda_B$ (pm)	Standard deviation (pm)	Standard deviation (cm)
0	0	0	0
10	3.88	0.64	2.62
20	8.25	0.46	1.89
30	12.13	0.64	2.62
40	16.38	0.52	2.13
50	20.50	0.53	2.17
60	24.50	0.53	2.17

From (4), it is possible to estimate the expected value for the wavelength variation versus the variation of the level of the water column. However, the parameter with more significant uncertainty is Young's modulus of the diaphragm, as it does not have constant parameters, especially in the epoxy resin concentration during the manufacturing process and fiber orientation. According to [33], Young's modulus values can range from 6.7 GPa to 78 GPa for CFRC. Using the value of 6.7 GPa, (4) predicts a variation in the wavelength of 6.4 pm for each 10 cm of the level of the water column, while the value of 78 GPa predicts a variation in the wavelength of 0.55 pm. Isolating the modulus of elasticity in (4), using a variation of 4.1 pm (same value of the linear coefficient shown in Fig. (4)), the value of 10.45 GPa is obtained for Young's modulus of the CPFRC diaphragm.

From Young's modulus value of 10.45 GPa and (4), it is possible to estimate the values obtained

by the level sensor for a variation of 60 cm in the water column, both for filling and draining the tube. The result of the simulated and experimental values (in addition to the temperature variation throughout the experiment) are shown in Fig. 5. The temperature curve shows minor variations around 23 °C, especially for 10 cm and 20 cm values. These variations occur for two reasons; the first is a mechanical oscillation when filling the tube at these initial values. The filling process consists of pouring, through the upper part of the tube, the amount of water equivalent to 10 cm of variation in the height of the water column. When hitting the diaphragm, the mechanical oscillations of the impact are transferred to the temperature sensor. This phenomenon is not observed for values greater than 20 cm because the water in the tube dampens these impacts. The other temperature variation observed throughout the experiment is due to the difference in temperature of the water and the diaphragm. The wavelength variation of the level sensor is compensated by the second FBG that works as a temperature sensor.

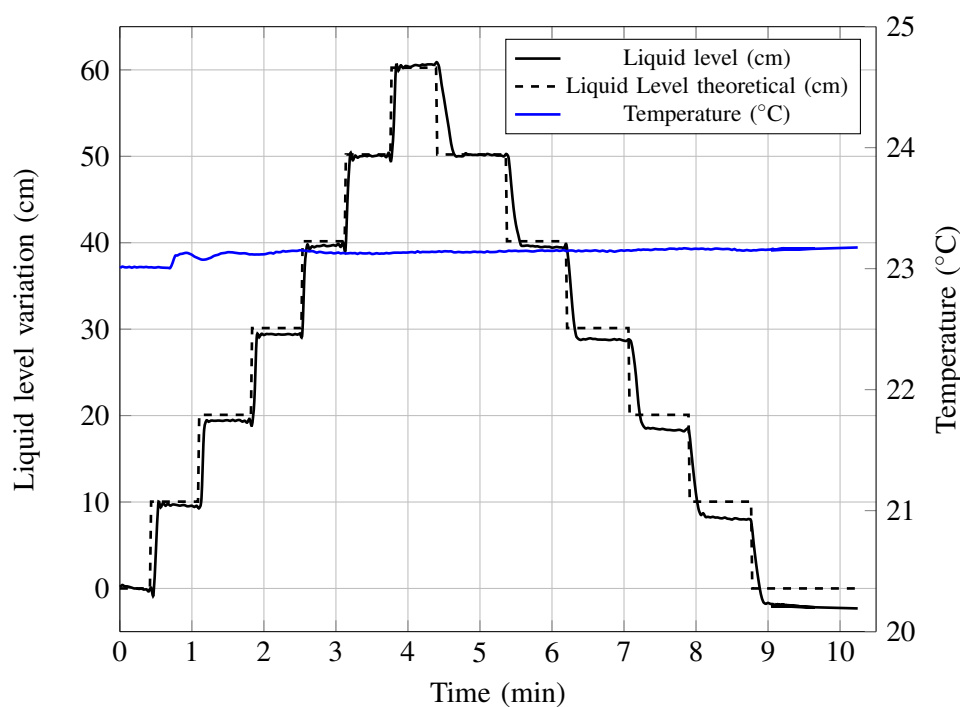


Fig. 5. Comparison of experimental liquid level and level measured by the proposed sensor.

During the increase of the water column, a maximum difference of 1.28 cm is observed between the theoretical and the experimental value for the heights of 30 cm and 40 cm. These values were already expected since they are within the standard deviation for their respective heights, according to Table I. However, the tube emptying process is not a process in which the experimental arrangement used allows precise control of how much the water column height decreases. This is because, as shown in Fig. 2, a valve is used to empty the tube, and its closing or opening leads to minor variations in the desired amount of water. This is more evident in Fig. 5 when at heights of 30 cm, 20 cm, 10 cm, and 0 cm, the level curve is not constant but a decreasing line. Even with this difficulty in maintaining the desired value while emptying the tube, the maximum difference between the simulated and experimental observed was 2.2 cm for a liquid-level of 10 cm. This value is smaller than the standard deviation obtained in Table 1, 2.62 cm, for the same height.

The encapsulation technique used in this paper is the main contribution and cannot be directly compared with previous papers. However, previous works also use a diaphragm for level or pressure measurement. In [28], the authors use an epoxy diaphragm with a sensitivity of 47.7 pm/kPa for a thickness of 1 mm. Converting the sensitivity of this work to pressure, the sensitivity obtained is 4.15 pm/kPa for a thickness of 3 mm. The lower sensitivity is due to the greater thickness and a material with a higher Young's modulus.

In [32], a carbon fiber diaphragm was used for level measurement. However, the encapsulation technique differs, with the sensor glued externally to the diaphragm. The sensitivity obtained was 1854 pm/cm, but with a thickness of 0.2 mm. This article used a thickness of 3 mm (the smallest that the manufacturing process can achieve) and a sensitivity of 4.1 pm/cm. Despite greater sensitivity, it is worth considering that the thickness used is 15 times smaller. According to (4), the difference between the two sensors is expected, as the relationship between strain and thickness is quadratic.

IV. CONCLUSION

This work uses a new FBG encapsulation technique for liquid-level measurement using CFRP. The sensor consists of a CFRP diaphragm with an embedded FBG whose pressure exerted by the diaphragm causes a deformation. From the FEM can determine that the center of the CFRP diaphragm is the point subject to major deformation. Because of this, the FBG sensor was embedded in the center of the diaphragm.

The calibration results show a linear behavior, with a 4.1 pm/cm slope and a correlation coefficient of $R^2 = 0.999$. From the equations presented in section II, it was possible to estimate Young's modulus of the CFRP fiber used, which was 10.45 GPa. Although water was used in the calibration process, other liquids could also be used, obtaining a different angular coefficient depending on the density of the liquid used.

V. ACKNOWLEDGMENTS

The authors acknowledge CAPES (Coordination of Superior Level Staff Improvement), CNPQ (National Council for Scientific and Technological Development), FINEP (Funding Authority for Studies and Projects), Araucária Foundation, and SETI (State Secretary of Science, Technology, and Higher Education of Paraná), and Multi-User Photonics Facility - UTFPR-CT. This study was financed in part by the Coordenação de Aperfeiçoamento de Pessoal de Nível Superior - Brasil (CAPES) - Finance Code 001.

REFERENCES

- [1] K. Hill and G. Meltz, "Fiber Bragg grating technology fundamentals and overview," *Journal of Lightwave Technology*, vol. 15, no. 8, pp. 1263–1276, 1997. [Online]. Available: <http://ieeexplore.ieee.org/document/618320/>
- [2] A. Othonos, "Fiber Bragg gratings," *Review of Scientific Instruments*, vol. 68, no. 12, pp. 4309–4341, 12 1997. [Online]. Available: <http://aip.scitation.org/doi/10.1063/1.1148392>
- [3] B. Lee, "Review of the present status of optical fiber sensors," *Optical Fiber Technology*, vol. 9, no. 2, pp. 57–79, 4 2003. [Online]. Available: <https://linkinghub.elsevier.com/retrieve/pii/S1068520002005278>
- [4] J. Chen, B. Liu, and H. Zhang, "Review of fiber Bragg grating sensor technology," *Frontiers of Optoelectronics in China*, vol. 4, no. 2, pp. 204–212, 2011.
- [5] A. Teixeira, M. Lima, O. Frazao, and J. Ferreira da Rocha, "Fiber Bragg gratings for telecommunications," in *Proceedings of 2001 3rd International Conference on Transparent Optical Networks (IEEE Cat. No.01EX488)*, pp. 127–130. [Online]. Available: <http://ieeexplore.ieee.org/document/934735/>

- [6] A. Méndez, “Fiber Bragg grating sensors: a market overview,” in *Third European Workshop on Optical Fibre Sensors*, vol. 6619, pp. 661 905–661 905, 7 2007. [Online]. Available: <http://proceedings.spiedigitallibrary.org/proceeding.aspx?articleid=1304726>
- [7] K. de Moraes Sousa, A. A. Hafner, E. G. Carati, H. J. Kalinowski, and J. C. C. da Silva, “Validation of thermal and electrical model for induction motors using fiber Bragg gratings,” *Measurement*, vol. 46, no. 6, pp. 1781–1790, 7 2013. [Online]. Available: <https://linkinghub.elsevier.com/retrieve/pii/S0263224113000468>
- [8] K. M. Sousa, I. Brutkowski Vieira da Costa, E. S. Maciel, J. E. Rocha, C. Martelli, and J. C. Cardozo da Silva, “Broken Bar Fault Detection in Induction Motor by Using Optical Fiber Strain Sensors,” *IEEE Sensors Journal*, vol. 17, no. 12, pp. 3669–3676, 6 2017. [Online]. Available: <http://ieeexplore.ieee.org/document/7904691/>
- [9] J. D. Pelegrin, U. J. Dreyer, K. M. Sousa, and J. Carlos, “Smart Carbon-Fiber Reinforced Polymer Optical Fiber Bragg Grating for Monitoring Fault Detection in Bearing,” *IEEE Sensors Journal*, vol. 22, no. 13, pp. 12921–12929, 2022.
- [10] B. Brusamarello, J. C. Cardozo da Silva, K. de Moraes Sousa, and G. A. Guarneri, “Bearing Fault Detection in Three-Phase Induction Motors Using Support Vector Machine and Fiber Bragg Grating,” *IEEE Sensors Journal*, vol. 23, no. 5, pp. 4413–4421, 3 2023. [Online]. Available: <https://ieeexplore.ieee.org/document/9757224/>
- [11] K. M. Sousa, U. J. Dreyer, C. Martelli, and J. C. Cardozo Da Silva, “Dynamic Eccentricity Induced in Induction Motor Detected by Optical Fiber Bragg Grating Strain Sensors,” *IEEE Sensors Journal*, vol. 16, no. 12, pp. 4786–4792, 2016.
- [12] M. M. Werneck, R. C. d. S. B. Allil, and B. A. Ribeiro, “Calibration and operation of a fibre Bragg grating temperature sensing system in a grid-connected hydrogenerator,” *IET Science, Measurement & Technology*, vol. 7, no. 1, pp. 59–68, 1 2013. [Online]. Available: <https://onlinelibrary.wiley.com/doi/10.1049/iet-smt.2012.0064>
- [13] U. J. Dreyer, F. Mezzadri, G. Dutra, T. da Silva, C. A. Bavastri, E. V. da Silva, C. Martelli, and J. C. C. da Silva, “Quasi-Distributed Optical Fiber Transducer for Simultaneous Temperature and Vibration Sensing in High-Power Generators,” *IEEE Sensors Journal*, vol. 18, no. 4, pp. 1547–1554, 2 2018. [Online]. Available: <http://ieeexplore.ieee.org/document/8240599/>
- [14] A. Kalinowski, R. P. Linessio, C. J. A. Mendonca, U. J. Dreyer, P. Antunes, A. Ramos, and J. C. C. d. Silva, “Fiber-Optic Bragg Grating Sensors for Biomechanical Analysis of Fracture Healing,” *IEEE Sensors Journal*, vol. 21, no. 21, pp. 24 177–24 184, 11 2021. [Online]. Available: <https://ieeexplore.ieee.org/document/9546778/>
- [15] A. B. Socorro-Leranz, S. Diaz, S. Castillo, U. J. Dreyer, C. Martelli, J. C. Cardozo da Silva, I. Uzqueda, M. Gomez, and C. R. Zamarreno, “Optical System Based on Multiplexed FBGs to Monitor Hand Movements,” *IEEE Sensors Journal*, vol. 21, no. 13, pp. 14 081–14 089, 7 2021. [Online]. Available: <https://ieeexplore.ieee.org/document/9118919/>
- [16] A. Kalinowski, R. P. Linessio, C. J. A. Mendonca, P. Antunes, A. Ramos, and J. C. C. d. Silva, “Noninvasive Optical Instrumentation for Bone Healing Process Analysis,” *IEEE Sensors Journal*, vol. 21, no. 13, pp. 14 060–14 068, 7 2021. [Online]. Available: <https://ieeexplore.ieee.org/document/9235569/>
- [17] M. D. Lavarda, D. F. Gomes, T. Paes, R. O. de Sousa, U. J. Dreyer, J. C. C. da Silva, and C. Martelli, “Smart Foot Based on FBG Integrated in Composite Material and Adaptive Fuzzy Controller,” *IEEE Sensors Letters*, vol. 7, no. 9, pp. 1–4, 9 2023. [Online]. Available: <https://ieeexplore.ieee.org/document/10230261/>
- [18] K. Loizou and E. Koutroulis, “Water level sensing: State of the art review and performance evaluation of a low-cost measurement system,” *Measurement*, vol. 89, pp. 204–214, 7 2016. [Online]. Available: <http://dx.doi.org/10.1016/j.measurement.2016.04.019https://linkinghub.elsevier.com/retrieve/pii/S0263224116300768>
- [19] H. Takahashi, N. M. Dung, K. Matsumoto, and I. Shimoyama, “Differential pressure sensor using a piezoresistive cantilever,” *Journal of Micromechanics and Microengineering*, vol. 22, no. 5, p. 055015, 5 2012. [Online]. Available: <https://iopscience.iop.org/article/10.1088/0960-1317/22/5/055015>
- [20] S.-W. Wang, C.-C. Chen, C.-M. Wu, and C.-M. Huang, “A continuous water-level sensor based on load cell and floating pipe,” in *2018 IEEE International Conference on Applied System Invention (ICASI)*, pp. 151–154, 4 2018. [Online]. Available: <https://ieeexplore.ieee.org/document/8394554/>
- [21] D. Brumbi, “Industrial Level Sensing with Radar,” *Frequenz*, vol. 60, no. 1-2, pp. 2–5, 1 2006. [Online]. Available: <https://www.degruyter.com/document/doi/10.1515/FREQ.2006.60.1-2.2/html>
- [22] C. A. Diaz, A. Leal-Junior, C. Marques, A. Frizzera, M. J. Pontes, P. F. Antunes, P. S. Andre, and M. R. Ribeiro, “Optical fiber sensing for sub-millimeter liquid-level monitoring: a review,” *IEEE Sensors Journal*, vol. 19, no. 17, pp. 7179–7191, 2019.
- [23] C.-f. B. Grating, H.-y. Chang, Y.-c. Chang, H.-j. Sheng, M.-y. Fu, W.-f. Liu, and R. Kashyap, “An Ultra-Sensitive Liquid-Level Indicator Based on,” *IEEE Photonics Technology Letters*, vol. 28, no. 3, pp. 268–271, 2016.
- [24] C. Mou, K. Zhou, Z. Yan, H. Fu, and L. Zhang, “Liquid level sensor based on an excessively tilted fibre grating,” *Optics Communications*, vol. 305, pp. 271–275, 2013. [Online]. Available: <http://dx.doi.org/10.1016/j.optcom.2013.05.019>

- [25] S. Khaliq, S. W. James, and R. P. Tatam, "Fiber-optic liquid-level sensor using a long-period grating," vol. 26, no. 16, pp. 2000–2002, 2001.
- [26] K. Ren, L. Ren, J. Liang, X. Kong, H. Ju, Y. Xu, and Z. Wu, "Online fabrication scheme of helical long-period fiber grating for liquid-level sensing," *Applied Optics*, vol. 55, no. 34, p. 9675, 2016.
- [27] S. A. Sopian, S. Ambran, L. P. Ong, P. N. S. S. Ja'afar, H. Mohamed, and N. M. Yusoff, "Liquid Level Monitoring With Single Layered Rubber Diaphragm Fibre Bragg Grating Sensor," in *2021 8th International Conference on Electrical Engineering, Computer Science and Informatics (EECSI)*, pp. 263–266, 10 2021. [Online]. Available: <https://ieeexplore.ieee.org/document/9624284/>
- [28] S.-C. Her and S.-Z. Weng, "Fiber Bragg Grating Pressure Sensor Integrated with Epoxy Diaphragm," *Sensors*, vol. 21, no. 9, p. 3199, 5 2021. [Online]. Available: <https://www.mdpi.com/1424-8220/21/9/3199>
- [29] E. Morais, M. J. Pontes, C. Marques, and A. Leal-Junior, "Liquid Level Sensor with Two FBGs Embedded in a PDMS Diaphragm: Analysis of the Linearity and Sensitivity," *Sensors*, vol. 22, no. 3, p. 1268, 2 2022. [Online]. Available: <https://www.mdpi.com/1424-8220/22/3/1268>
- [30] J. R. Galvão, C. R. Zamarreño, C. Martelli, J. C. Cardozo Da Silva, F. J. Arregui, and I. R. Matías, "Smart Carbon Fiber Transtibial Prosthesis Based on Embedded Fiber Bragg Gratings," *IEEE Sensors Journal*, vol. 18, no. 4, pp. 1520–1527, 2018.
- [31] G. G. Kuhn, K. M. Sousa, C. Martelli, C. A. Bavastri, and J. C. C. D. Silva, "Embedded FBG Sensors in Carbon Fiber for Vibration and Temperature Measurement in Power Transformer Iron Core," *IEEE Sensors Journal*, vol. 20, no. 22, pp. 13 403–13 410, 2020.
- [32] D. Song, "Liquid-level sensor using a fiber Bragg grating and carbon fiber composite diaphragm," *Optical Engineering*, vol. 50, no. 1, p. 014401, 2011.
- [33] H. Rahmani, S. H. Mahmoudi, A. Ashori, and M. Golriz, "Elastic Properties of Carbon Fibre-Reinforced Epoxy Composites," *Polymers and Polymer Composites*, vol. 23, no. 7, pp. 475–482, 2015.